

Unified Scattering and Photoluminescence Spectra for Strong Plasmon-Exciton Coupling

Yijie Niu,^{1,2} Hongxing Xu^{1,2} and Hong Wei^{1,3,*}

¹*Beijing National Laboratory for Condensed Matter Physics, Institute of Physics, Chinese Academy of Sciences, Beijing 100190, China*

²*School of Physics and Technology, Center for Nanoscience and Nanotechnology, and Key Laboratory of Artificial Micro- and Nano-structures of Ministry of Education, Wuhan University, Wuhan 430072, China*

³*Songshan Lake Materials Laboratory, Dongguan 523808, China*



(Received 9 August 2021; accepted 10 March 2022; published 21 April 2022)

The strong coupling between excitons and single plasmonic nanocavities enables plexcitonic states in nanoscale systems at room temperature. Here we demonstrate the strong coupling of surface plasmon modes of metal nanowires and excitons in monolayer semiconductors, with Rabi splitting manifested in both scattering and photoluminescence (PL) spectra. By utilizing the propagation properties of surface plasmons on the nanowires, the PL emitted through the scattering of plasmon-exciton hybrid modes is extracted. The analytically calculated scattering and PL spectra well reproduce the experimental results. These findings unify the scattering and PL spectra in the plexcitonic system and eliminate the ambiguities of PL emission, shedding new light on understanding the rich spectral phenomena in the plasmon-exciton strong coupling regime.

DOI: [10.1103/PhysRevLett.128.167402](https://doi.org/10.1103/PhysRevLett.128.167402)

Strong coupling between light and matter is a fundamental quantum optics phenomenon which has attracted considerable attention. For a quantum emitter coupling with an optical cavity, when the coherent energy exchange rate between them is sufficiently larger than their respective damping rate, the strong coupling is achieved with exciton polariton states formed [1]. The exciton polaritons possess extraordinary properties due to their mixed nature of light and matter, and can be exploited for various applications, such as Bose-Einstein condensation [2], lasing [3], topological insulator [4], and quantum information technologies [5–7]. The realization of strong coupling relies on the large coupling strength and low damping loss. The coupling strength is proportional to $\sqrt{N/V}$, where N is the effective number of excitons and V is the cavity mode volume. For the traditional optical cavities, strong coupling has been demonstrated in various systems [8–10], but it is hard to further enhance the coupling strength by reducing V due to diffraction limit. Alternatively, plasmonic nanocavities offer a straightforward way to realize strong plasmon-exciton coupling by confining electromagnetic field down to nanoscale spaces due to the excitation of surface plasmons (SPs) [11–22]. The much smaller mode volume of plasmonic nanocavities results in higher coupling strength, rendering strong coupling at room temperature. Even the strong coupling at single exciton level has been demonstrated [15,18–21].

The plasmon-exciton strong coupling was mostly investigated by using dark-field scattering, reflection, and transmission spectroscopy, and only a few experiments measured PL spectra. For single quantum dots coupled to

plasmonic nanostructures, obvious spectral splitting of PL has been observed [19–21], while for molecules, J aggregates, and two-dimensional transition metal dichalcogenides, PL from lower plexciton state or PL spectral broadening was mainly observed [23–30]. The origin of the PL spectral profiles of those plasmonic strong coupling systems remains ambiguous. In the coupled system, part of the PL is emitted through the radiation of SP modes, which can modulate the PL spectra as has been demonstrated in SP modified spontaneous emission [31,32]. In addition, the PL from the excitons not coupling with the plasmonic structure can also contribute to the detected PL signal. Because of the complexity of the PL emission process, it is more difficult to extract the strong coupling information from PL spectra. Separating the PL emission through the radiation of SP modes (SP-exciton hybrid modes) from the direct PL emission can help unveil the strong-coupling induced spectral features of PL.

In this Letter, we investigate the strong coupling between single Ag nanowires (NWs) and monolayer WSe₂ at ambient conditions by scattering and PL spectra. The peak splitting in scattering spectra due to strong coupling of two SP modes and excitons is observed, and Rabi splitting of 67 meV between adjacent plexciton branches is achieved. By separating the excitation and detection sites, the spectra of PL emitted through the scattering process of SP-exciton hybrid modes are obtained. The PL spectra normalized by that of pristine WSe₂ show the same profiles as the scattering spectra. The analytical results obtained by coupled-oscillators model well reproduce the experimental data of both scattering and PL. These results corroborate

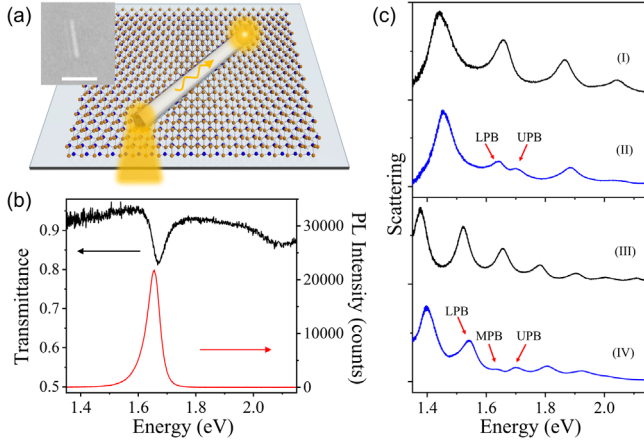


FIG. 1. (a) Schematic and optical microscopy image of a single Ag NW on monolayer WSe₂. The scale bar is 2 μm . (b) Transmission and PL spectra of a WSe₂ monolayer on glass substrate. (c) Scattering spectra of Ag NWs without (I, III) and with (II, IV) WSe₂. The plexciton peaks are marked with red arrows.

that scattering and PL are two aspects of the same strong coupling phenomenon, and provide deeper understanding on the PL spectra in plexcitonic systems.

The coupled system is composed of a Ag NW and monolayer WSe₂ [Fig. 1(a)]. The monolayer WSe₂ grown by chemical vapor deposition method was firstly transferred to glass substrate by a wet transfer method (see Sec. 1 in the Supplemental Material [33]). After dispersing the chemically synthesized Ag NWs (diameter about 90 ± 10 nm) by spin coating, an Al₂O₃ layer of 5 nm thickness was deposited onto the sample surface. Figure 1(b) shows the transmission and PL spectra of a WSe₂ monolayer on glass substrate [22]. The energy of the transmission dip E_0 is about 1.672 eV and linewidth γ_0 is about 50 meV according to a Lorentzian fit. To excite propagating SPs on the Ag NW, supercontinuum laser light was focused onto one end of the NW from the glass side through an oil immersion objective (100 \times , NA 1.49). The emitted light from the opposite end of the NW was collected by the same objective and directed to a spectrometer.

The Ag NW can be regarded as a Fabry-Pérot resonator supporting high order SP modes [37]. Figure 1(c) shows the scattering spectra of Ag NWs without and with monolayer WSe₂. When the Ag NW length is shorter (~ 1.2 μm), there are only four SP modes in the spectral range of 1.35 to 2.15 eV [Fig. 1(c) I]. The energy difference between adjacent SP modes is large enough, so that only one SP mode couples with the excitons. For the Ag NW on monolayer WSe₂, the lower plexciton branch (LPB) and upper plexciton branch (UPB) resulting from the strong coupling of a SP mode and excitons are clearly observed [Fig. 1(c) II]. With the increase of Ag NW length (~ 2 μm), the SP modes redshift and additional peaks appear at higher energy, leading to decreased energy difference between adjacent SP modes [Fig. 1(c) III].

When two adjacent SP modes have spectral overlaps with the excitons, three peaks are observed, which can be assigned to the LPB, middle plexciton branch (MPB), and UPB, respectively [Fig. 1(c) IV].

The spectral range for two SP modes coupling with excitons can be described by a three-coupled-oscillators model [38–41]:

$$\begin{pmatrix} E_1 - \frac{i\gamma_1}{2} & 0 & g_1 \\ 0 & E_2 - \frac{i\gamma_2}{2} & g_2 \\ g_1 & g_2 & E_0 - \frac{i\gamma_0}{2} \end{pmatrix} \begin{pmatrix} \alpha \\ \beta \\ \varphi \end{pmatrix} = E \begin{pmatrix} \alpha \\ \beta \\ \varphi \end{pmatrix}, \quad (1)$$

where E_1 , E_2 , and E_0 are the energies of the lower energy plasmon (LEP) mode, higher energy plasmon (HEP) mode, and exciton, respectively; γ_1 , γ_2 , and γ_0 are the linewidths corresponding to E_1 , E_2 , and E_0 , respectively; g_1 and g_2 are the coupling strengths of LEP mode with exciton and HEP mode with exciton, respectively; E is the eigenvalue of the energy for corresponding plexcitons; α , β , and φ are the Hopfield coefficients which satisfy $|\alpha|^2 + |\beta|^2 + |\varphi|^2 = 1$.

The equations of motion for the three oscillators can be given by [41,42]

$$\begin{aligned} \ddot{x}_1 + \gamma_1 \dot{x}_1 + \omega_1^2 x_1 + 2g_1 \dot{x}_0 &= F_1(t), \\ \ddot{x}_2 + \gamma_2 \dot{x}_2 + \omega_2^2 x_2 + 2g_2 \dot{x}_0 &= F_2(t), \\ \ddot{x}_0 + \gamma_0 \dot{x}_0 + \omega_0^2 x_0 - 2g_1 \dot{x}_1 - 2g_2 \dot{x}_2 &= 0, \end{aligned} \quad (2)$$

where x_1 , x_2 , and x_0 are the coordinates of oscillations of the LEP mode, HEP mode, and exciton, respectively; ω_1 , ω_2 , and ω_0 are the frequencies of the LEP mode, HEP mode, and exciton, respectively; $F_1(t) = F_1 e^{-i\omega t}$ and $F_2(t) = F_2 e^{-i\omega t}$ are the driving forces due to external electromagnetic field. According to Eq. (2) and Larmor formula of dipole radiation, the intensity of scattered light can be expressed as (see Sec. 2 in the Supplemental Material [33]):

$$I_{\text{scat}}(\omega) \propto \omega^4 |x_1|^2 + \omega^4 |x_2|^2. \quad (3)$$

Figure 2(a) shows a series of scattering spectra for Ag NWs on monolayer WSe₂. The SP modes have an overall redshift from bottom to top, which can be induced by the change of diameter and length of Ag NWs (see Sec. 3 in the Supplemental Material [33]). The spectral sections showing Rabi splitting in Fig. 2(a) are plotted in Fig. 2(b). When the LEP mode is close to the exciton energy, strong coupling between LEP mode and exciton occurs [bottom spectrum in Fig. 2(b)]. When the SP modes redshift until the HEP mode matches with the exciton, strong coupling between HEP mode and exciton is obtained [top spectrum in Fig. 2(b)]. In the course of SP resonances redshift, the spectra show intermixed LEP-exciton-HEP interaction. The scattering spectra in Fig. 2(b) are fitted by Eq. (3), and the fitting

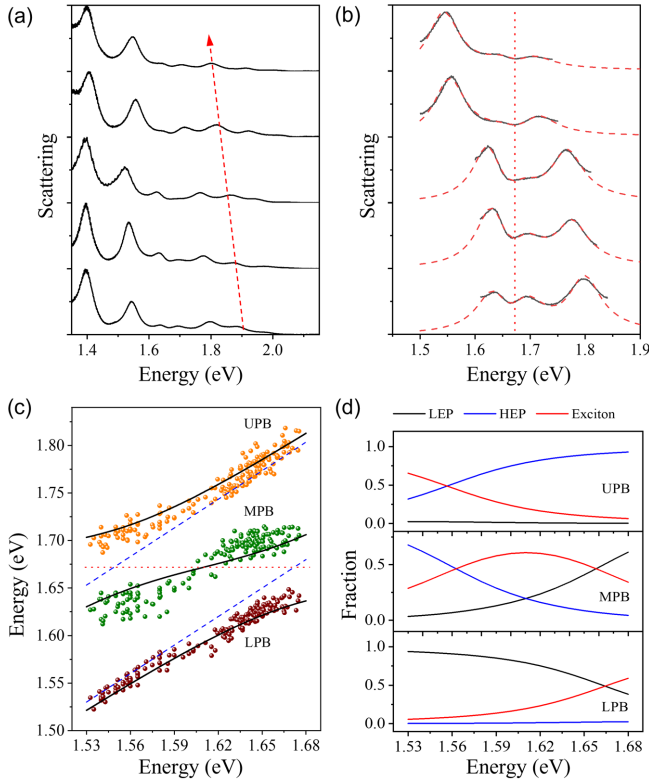


FIG. 2. (a) Scattering spectra of Ag NWs on monolayer WSe₂. The redshift is marked with the red arrow. (b) Magnified view of the spectra in (a) showing peak splits (black lines). The red dashed lines are the fitting results by Eq. (3). The red dot line indicates the transmission dip energy of exciton. (c) The energies of UPB (orange), MPB (green), and LPB (wine) as a function of the energy of LEP mode E_1 . The black lines are calculated by Eq. (1) with coupling strength of $g_1 = g_2 = 35$ meV. The blue dashed lines show the energy of LEP (E_1) and HEP (E_2) extracted from Eq. (3). The red dot line indicates the transmission dip energy of exciton. (d) Hopfield coefficients for LEP, HEP, and exciton contributions to UPB, MPB, and LPB as a function of E_1 .

results (red dashed lines) agree very well with the experimental results. The energies of the two SP modes E_1 and E_2 obtained by fitting the scattering spectra using Eq. (3) show a linear relationship (see Sec. 4 in the Supplemental Material [33]).

To ensure that the coupled system is in the strong coupling regime, we analyze its anticrossing behavior. Figure 2(c) shows the experimental and analytical results of three plexciton branches as a function of the LEP energy E_1 . The experimental eigenenergies of UPB, MPB, and LPB are obtained by utilizing three Lorentzian peaks to fit the scattering spectra. Then by adjusting the coupling strength g_1 and g_2 and solving Eq. (1), the eigenvalues of the plexciton branches are obtained [black lines in Fig. 2(c)]. When $g_1 = g_2 = 35$ meV, the calculated anticrossing dispersions agree well with the experimental results. In experiments, we measured the scattering spectra of Ag NWs on glass substrate which have similar length and same

number of SP modes as those Ag NWs on WSe₂, and obtained the linewidth of LEP and HEP modes, $\gamma_1 \approx \gamma_2 \approx 60$ meV. According to the calculation results, the minimal Rabi splitting between UPB and MPB is about $\Omega_{\text{UPB-MPB}} \approx 67$ meV $> (\gamma_2 + \gamma_0)/2$, and the minimal Rabi splitting between MPB and LPB is about $\Omega_{\text{MPB-LPB}} \approx 67$ meV $> (\gamma_1 + \gamma_0)/2$, satisfying the strong coupling criterion.

In order to quantitatively analyze the hybridization, we calculate the Hopfield coefficients for three branches [43], as shown in Fig. 2(d). For the UPB, the weight of LEP is always a very small value, which indicates that the hybridization mainly results from the contribution of HEP and exciton. Likewise, for the LPB, the hybridization mainly results from the contribution of LEP and exciton. However, a strong hybridization of LEP, HEP, and exciton is observed for the MPB, leading to the formation of a mixed state of part-LEP, part-HEP, and part exciton. When the LEP (HEP) energy matches the exciton energy, the detuning between the HEP (LEP) mode and exciton is so large that the experimental results can be well fitted by the two-coupled-oscillators model (see Sec. 5 in the Supplemental Material [33]). This also explains the slight deviation between experimental and calculation results for the MPB in Fig. 2(c).

To measure the PL spectra, the coupled system was excited by focusing laser light of 532 nm wavelength at one end of the Ag NW with the polarization perpendicular to the NW, and the PL was collected at the opposite end of the NW. Under this configuration, the background PL from uncoupled excitons is suppressed (see Sec. 6 in the Supplemental Material [33]). Figures 3(a) and 3(d) show the PL spectra when LEP mode is close to exciton and HEP mode is close to exciton, respectively. Compared with the PL spectra of bare WSe₂, peak shift and broadening are observed, and an additional peak appears at the lower energy side (see Sec. 7 in the Supplemental Material [33]). Figures 3(b) and 3(e) show the results of the PL spectra in Figs. 3(a) and 3(d) divided by the corresponding PL spectra of bare WSe₂, respectively. Interestingly, the normalized PL spectra show the same profiles as the corresponding scattering spectra in Figs. 3(c) and 3(f). These results indicate that the reshaped PL spectra are caused not only by the modulation of SP resonances, but also by the plasmon-exciton strong coupling.

The PL spectra are fitted by three Lorentzian peaks [Figs. 3(a) and 3(d)]. The peak energies of the fitting results for the PL spectra are plotted as a function of the LEP energy E_1 [solid dots in Fig. 4(a)]. Considering the similarity of the normalized PL spectra and scattering spectra as shown in Fig. 3, we calculate the PL spectra through multiplying the scattering spectra calculated according to Eq. (3) by the Lorentzian fitted PL spectrum of bare WSe₂ (see Sec. 8 in the Supplemental Material [33]). The calculated PL spectra are fitted by four Lorentzian peaks and the fitting results are shown in

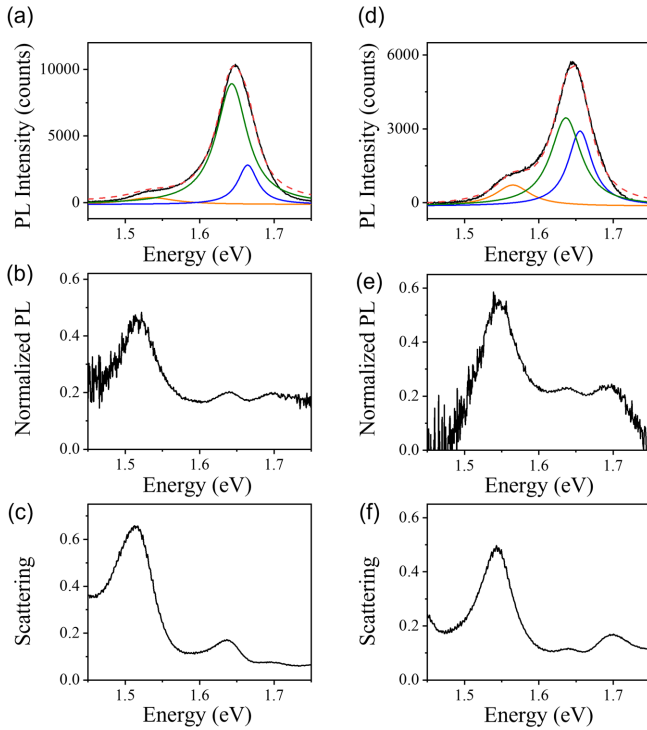


FIG. 3. (a) PL spectrum for a hybrid system of Ag NW and monolayer WSe₂ when LEP energy is close to exciton energy ($E_1 = 1.6456$ eV and $E_2 = 1.7996$ eV). The red dashed line is obtained by fitting the spectrum using three Lorentzian peaks (orange, green, and blue lines). (b) Normalized PL spectrum resulting from dividing the spectrum in (a) by the PL spectrum of the bare WSe₂. (c) Scattering spectrum for the same NW in (a). (d)–(f) The same as (a)–(c) but for a hybrid system with HEP energy close to exciton energy ($E_1 = 1.545$ eV, $E_2 = 1.67$ eV).

Fig. 4(a) as hollow dots connected by short lines. As can be seen, the theoretical results of orange dots in the lower energy range and green dots agree well with the experimental results. The energy of the experimental blue dots keeps almost constant in the whole energy range and is

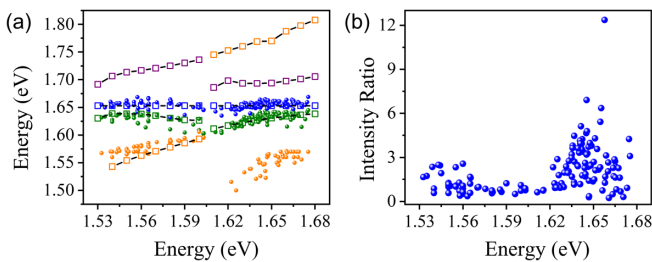


FIG. 4. (a) The energies of fitting peaks in the experimental (solid dots) and calculated (hollow square dots) PL spectra as a function of E_1 . The orange, green, and blue solid dots correspond to three fitting peaks for experimental PL spectra. The orange, green, blue, and purple hollow dots correspond to four fitting peaks for calculated PL spectra. (b) Experimental results of the integrated intensity ratio between the plexcitons corresponding to solid green dots in panel (a) and excitons as a function of E_1 .

close to the pristine exciton emission peak. The spectral peaks corresponding to the experimental orange dots in the higher energy range are not included in the theoretical calculation. The calculated orange dots in the higher energy range and the purple dots are close to the energies of the corresponding scattering peaks [see Fig. S12(c) in the Supplemental Material [33]]. The Rabi splitting obtained from the calculated PL results is about 61 meV for $E_1 \approx 1.53$ eV, and 63 meV for $E_1 \approx 1.65$ eV, respectively. Although we cannot obtain the plexciton peaks of higher energy by fitting the experimental PL spectra, the agreement of the normalized PL spectra and scattering spectra indicates the existence of higher energy plexciton component in the PL spectra. Figure 4(b) shows the integrated intensity ratio between the plexcitons corresponding to the solid green dots and excitons, which reaches maximum when the energy of the SP mode is close to the exciton energy (~ 1.65 eV for PL peak). The data in the lower and higher energy range in Fig. 4 can be considered as the results of two oscillators coupling (i.e., one SP mode coupling with excitons), due to the small contribution of the other SP mode.

In summary, the strong coupling of SPs and excitons in the coupled system of Ag NWs and monolayer WSe₂ is investigated by scattering and PL spectra. The strong coupling of one or two SP modes and excitons is demonstrated in the scattering spectra. Because of the long propagation length of SPs on Ag NWs, the excitation and collection regions can be spatially separated, which is utilized to extract the PL emitted through the scattering of SP-exciton hybrid modes. It is found that the PL and scattering light share the same spectral profiles resulting from strong coupling. The analytical calculation results agree with the experimental data. These results clarify the correlative scattering and PL processes and offer new perspective on the spectral responses of plasmon-exciton strong coupling systems.

This work was supported by the National Natural Science Foundation of China (Grants No. 12074421, No. 11774413, and No. 91850207), and the Strategic Priority Research Program of Chinese Academy of Sciences (Grant No. XDB33000000). We thank the Laboratory of Microfabrication in Institute of Physics, Chinese Academy of Sciences for the experimental support.

*weihong@iphy.ac.cn

- [1] G. Khitrova, H. M. Gibbs, M. Kira, S. W. Koch, and A. Scherer, *Nat. Phys.* **2**, 81 (2006).
- [2] J. Kasprzak, M. Richard, S. Kundermann, A. Baas, P. Jeambrun, J. M. J. Keeling, F. M. Marchetti, M. H. Szymańska, R. André, J. L. Staehli, V. Savona, P. B. Littlewood, B. Deveaud, and L. S. Dang, *Nature (London)* **443**, 409 (2006).

- [3] S. Kéna-Cohen and S. R. Forrest, *Nat. Photonics* **4**, 371 (2010).
- [4] S. Klembt, T. H. Harder, O. A. Egorov, K. Winkler, R. Ge, M. A. Bandres, M. Emmerling, L. Worschech, T. C. H. Liew, M. Segev, C. Schneider, and S. Höfling, *Nature (London)* **562**, 552 (2018).
- [5] A. Imamoğlu, D. D. Awschalom, G. Burkard, D. P. DiVincenzo, D. Loss, M. Sherwin, and A. Small, *Phys. Rev. Lett.* **83**, 4204 (1999).
- [6] A. Amo, T. C. H. Liew, C. Adrados, R. Houdré, E. Giacobino, A. V. Kavokin, and A. Bramati, *Nat. Photonics* **4**, 361 (2010).
- [7] D. E. Chang, V. Vuletić, and M. D. Lukin, *Nat. Photonics* **8**, 685 (2014).
- [8] J. P. Reithmaier, G. Şek, A. Löffler, C. Hofmann, S. Kuhn, S. Reitzenstein, L. V. Keldysh, V. D. Kulakovskii, T. L. Reinecke, and A. Forchel, *Nature (London)* **432**, 197 (2004).
- [9] X. Z. Liu, T. Galfsky, Z. Sun, F. N. Xia, E.-c. Lin, Y.-H. Lee, S. Kéna-Cohen, and V. M. Menon, *Nat. Photonics* **9**, 30 (2015).
- [10] L. Zhang, R. Gogna, W. Burg, E. Tutuc, and H. Deng, *Nat. Commun.* **9**, 713 (2018).
- [11] H. Wei, X. H. Yan, Y. J. Niu, Q. Li, Z. L. Jia, and H. X. Xu, *Adv. Funct. Mater.* **31**, 2100889 (2021).
- [12] A. E. Schlather, N. Large, A. S. Urban, P. Nordlander, and N. J. Halas, *Nano Lett.* **13**, 3281 (2013).
- [13] G. Zengin, M. Wersäll, S. Nilsson, T. J. Antosiewicz, M. Käll, and T. Shegai, *Phys. Rev. Lett.* **114**, 157401 (2015).
- [14] K. Santhosh, O. Bitton, L. Chuntonov, and G. Haran, *Nat. Commun.* **7**, 11823 (2016).
- [15] R. Chikkaraddy, B. de Nijs, F. Benz, S. J. Barrow, O. A. Scherman, E. Rosta, A. Demetriadou, P. Fox, O. Hess, and J. J. Baumberg, *Nature (London)* **535**, 127 (2016).
- [16] D. Zheng, S. P. Zhang, Q. Deng, M. Kang, P. Nordlander, and H. X. Xu, *Nano Lett.* **17**, 3809 (2017).
- [17] J. X. Wen, H. Wang, W. L. Wang, Z. X. Deng, C. Zhuang, Y. Zhang, F. Liu, J. C. She, J. Chen, H. J. Chen, S. Z. Deng, and N. S. Xu, *Nano Lett.* **17**, 4689 (2017).
- [18] R. Liu, Z. K. Zhou, Y. C. Yu, T. W. Zhang, H. Wang, G. H. Liu, Y. Wei, H. J. Chen, and X. H. Wang, *Phys. Rev. Lett.* **118**, 237401 (2017).
- [19] H. Groß, J. M. Hamm, T. Tufarelli, O. Hess, and B. Hecht, *Sci. Adv.* **4**, eaar4906 (2018).
- [20] H. Leng, B. Szychowski, M. C. Daniel, and M. Pelton, *Nat. Commun.* **9**, 4012 (2018).
- [21] K. D. Park, M. A. May, H. X. Leng, J. R. Wang, J. A. Kropp, T. Gougousi, M. Pelton, and M. B. Raschke, *Sci. Adv.* **5**, eaav5931 (2019).
- [22] X. H. Yan and H. Wei, *Nanoscale* **12**, 9708 (2020).
- [23] S. R. K. Rodriguez, J. Feist, M. A. Verschuuren, F. J. Garcia Vidal, and J. Gómez Rivas, *Phys. Rev. Lett.* **111**, 166802 (2013).
- [24] J. Bellessa, C. Bonnand, J. C. Plenet, and J. Mugnier, *Phys. Rev. Lett.* **93**, 036404 (2004).
- [25] M. Wersäll, J. Cuadra, T. J. Antosiewicz, S. Balci, and T. Shegai, *Nano Lett.* **17**, 551 (2017).
- [26] M. Wersäll, B. Munkhbat, D. G. Baranov, F. Herrera, J. Cao, T. J. Antosiewicz, and T. Shegai, *ACS Photonics* **6**, 2570 (2019).
- [27] S. J. Wang, S. L. Li, T. Chervy, A. Shalabney, S. Azzini, E. Orgiu, J. A. Hutchison, C. Genet, P. Samorì, and T. W. Ebbesen, *Nano Lett.* **16**, 4368 (2016).
- [28] M. E. Kleemann, R. Chikkaraddy, E. M. Alexeev, D. Kos, C. Carnegie, W. Deacon, A. C. de Pury, C. Grosse, B. de Nijs, J. Mertens, A. I. Tartakovskii, and J. J. Baumberg, *Nat. Commun.* **8**, 1296 (2017).
- [29] J. Qin, Y. H. Chen, Z. Zhang, Y. Zhang, R. J. Blaikie, B. Ding, and M. Qiu, *Phys. Rev. Lett.* **124**, 063902 (2020).
- [30] Y. Jiang, H. Wang, S. Wen, H. Chen, and S. Deng, *ACS Nano* **14**, 13841 (2020).
- [31] M. Ringler, A. Schwemer, M. Wunderlich, A. Nichtl, K. Kürzinger, T. A. Klar, and J. Feldmann, *Phys. Rev. Lett.* **100**, 203002 (2008).
- [32] L. Zhao, T. Ming, H. Chen, Y. Liang, and J. Wang, *Nanoscale* **3**, 3849 (2011).
- [33] See Supplemental Material at <http://link.aps.org/supplemental/10.1103/PhysRevLett.128.167402> for experimental details and further analyses, which includes Refs. [34–36].
- [34] Y. Sun and Y. Xia, *Adv. Mater.* **14**, 833 (2002).
- [35] A. Hohenau, P. Kusar, C. Gruber, and J. R. Krenn, *Opt. Lett.* **37**, 746 (2012).
- [36] D. E. Chang, A. S. Sørensen, P. R. Hemmer, and M. D. Lukin, *Phys. Rev. B* **76**, 035420 (2007).
- [37] H. Ditlbacher, A. Hohenau, D. Wagner, U. Kreibig, M. Rogers, F. Hofer, F. R. Aussenegg, and J. R. Krenn, *Phys. Rev. Lett.* **95**, 257403 (2005).
- [38] N. I. Cade, T. Ritman-Meer, and D. Richards, *Phys. Rev. B* **79**, 241404(R) (2009).
- [39] H. Yang, J. Yao, X.-W. Wu, D.-J. Wu, and X.-J. Liu, *J. Phys. Chem. C* **121**, 25455 (2017).
- [40] J. Cuadra, D. G. Baranov, M. Wersäll, R. Verre, T. J. Antosiewicz, and T. Shegai, *Nano Lett.* **18**, 1777 (2018).
- [41] B. Munkhbat, D. G. Baranov, A. Bisht, M. A. Hoque, B. Karpik, S. P. Dash, and T. Shegai, *ACS Nano* **14**, 1196 (2020).
- [42] X. H. Wu, S. K. Gray, and M. Pelton, *Opt. Express* **18**, 23633 (2010).
- [43] B. W. Li, S. Zu, Z. P. Zhang, L. H. Zheng, Q. Jiang, B. W. Du, Y. Luo, Y. J. Gong, Y. F. Zhang, F. Lin, B. Shen, X. Zhu, P. M. Ajayan, and Z. Y. Fang, *Opto-Electron. Adv.* **2**, 190008 (2019).